PERGAMON

Journal of the Mechanics and Physics of Solids
49 (2001) 1639–1663

JOURNAL OF THE
MECHANICS AND
PHYSICS OF SOLIDS

www.elsevier.com/locate/jmps

Microstructure-sensitive design of a compliant beam

B.L. Adams[a,*], A. Henrie[a], B. Henrie[a], M. Lyon[a], S.R. Kalidindi[b], H. Garmestani[c]

[a] *Department of Mechanical Engineering, Brigham Young University, PO Box 24201, Provo, UT 84602, USA*
[b] *Department of Materials Engineering, Drexel University, Philadelphia, PA 19104, USA*
[c] *Department of Mechanical Engineering at FAMU-FSU College of Engineering, Tallahassee, FL 32310, USA*

Received 17 July 2000; received in revised form 29 January 2001

Abstract

We show that mechanical design can be conducted where consideration of polycrystalline microstructure as a continuous design variable is facilitated by use of a spectral representation space. Design of a compliant fixed-guided beam is used as a case study to illustrate the main tenets of the new approach, called microstructure-sensitive design (MSD). Selection of the mechanical framework for the design (e.g., mechanical constitutive model) dictates the dimensionality of the pertinent representation. Microstructure is considered to be comprised of basic elements that belong to the material set. For the compliant beam problem, these are uni-axial distribution functions. The universe of pertinent microstructures is found to be the convex hull of the material set, and is named the material hull. Design performance, in terms of specified design objectives and constraints, is represented by one or more surfaces (often hyperplanes) of finite dimension that intersect the material hull. Thus, the full range of microstructure, and concomitant design performance, can be exploited for any material class. Optimal placement of the salient iso-property surfaces within the material hull dictates the optimal set of microstructures for the problem. Extensions of MSD to highly constrained design problems of higher dimension is also described.

Keywords: A. Microstructures; B. Polycrystalline material; C. Optimization; D. Processing

* Corresponding author. Fax: +1-801-378-5037.
E-mail address: b_l_adams@byu.edu (B.L. Adams).

0022-5096/01/$ - see front matter
PII: S0022-5096(01)00016-3

1. Introduction

A central aim of materials science and engineering has been to discover and understand the important associations between the properties and performance of materials, their microstructures, and the processing methods required to achieve them—and then to exploit these in the design of engineered components. As an ideal, the flow of information would be in the direction: *design* → *properties* → *microstructure* → *processing*.

Considerable progress has been achieved in recent years, in facilitating this ideal direction of information flow, for problems where the topological features of internal structure control design performance. In several cases design objectives/constraints have been carried through to microstructure design and to the manufacture of these structures. For example, materials that realize extremal thermal expansion characteristics (including negative thermal expansion) have been studied by Sigmund and Torquato (1996). Compliant micromechanisms and structures with negative Poisson's ratios were studied and fabricated (Larsen et al., 1997). A more sophisticated problem, involving both geometrical optimization and the orientational characteristics of piezocrystals in hydrophone applications, has been reported by Sigmund et al. (1998). Microstructure optimization for microactuators, based upon the martensitic transformation, has been considered by Bhattacharya and James (1999). A recent survey of variational methods for optimization of structures and microstructures, focused mainly on topology optimization, is presented in the recent monograph of Cherkaev (2000).

The present work is aimed at facilitating the same ideal flow direction in the design paradigm, but it differs in its focus on the crystallographic and orientational attributes of polycrystalline microstructure, rather than on the topological. Related to this approach there has also been considerable progress in both innovative processing to realize novel microstructures, and in understanding the concomitant microstructure-properties associations. (References to this work are provided in Section 4.) However, at this juncture, the discipline has mainly communicated in the opposite direction to the ideal; i.e., *processing* → *microstructure* → *properties* → *design.* One important consequence is that design practice is usually constrained to the set of reported property values (e.g., in handbooks), without consideration of the broader set of properties that can be realized by the engineering of microstructure and processing. These limitations are most evident in design problems of a highly constrained nature, where multiple objectives and constraints are manifest, and where limitations in material properties are most keenly felt.

This paper is about mechanical design, and the means whereby the variability of the orientational aspects of microstructure can be fully considered in the design process, and the optimal direction of information flow can be realized. The new approach presented here is called microstructure-sensitive design (MSD). Crystalline materials are the main consideration, including metal and ceramic alloys and crystalline polymers. Thus a large segment of design practice is potentially impacted. In Section 4 extensions of the work to include spatial correlation information are described. Such extensions are anticipated to make a closer connection of the present work with the topological optimization methods being pursued by other investigators.

2. Microstructure sensitive design: basics

The roots of MSD trace back to the spectral representation of crystallographic texture. Specifically, the orientation distribution function (ODF) can be described as a Fourier series of generalized spherical harmonics, weighted by appropriate coefficients (Bunge, 1965; Roe, 1965). These harmonics form a complete orthonormal basis on the special orthogonal group in three dimensions, SO(3). In the approach taken by Bunge (1982), the harmonics are further symmetrized for the crystal symmetry subgroup, G, such that they form a basis for the homogeneous space SO(3)/G. This homogeneous space describes the complete set of physically distinctive orientations of the crystal phase (cf. Brocker and tom Dieck, 1985; Adams and Olson, 1998). Here, SO(3)/G shall be an example of a *fundamental zone*, which contains the building blocks from which microstructure is constructed. In contrast to the traditional representations of the fundamental zone, such as by points in an asymmetrical zone in the three-dimensional euler-angle space (cf. Bunge, 1982) or in Rodrigues space (cf. Sutton and Balluffi, 1995), here we choose a spectral representation in the infinite-dimensional Fourier space. In this context, the coordinates of any particular point are from the set of Fourier coefficients that describe the single orientation associated with that point. When the spectral representation of the fundamental zone is chosen, it is called a *material set*, in order to distinguish it from previous types of representations. Material sets of interest are of both greater and lesser complexity, as compared to SO(3)/G. As it shall be demonstrated, the particular material set(s) of interest in design is fully dictated by the mechanics and physics chosen to model material behavior.

Having represented the material set in the Fourier space, we realize the profound advantage that the universe of all microstructures, pertaining to the selected physical framework of the problem, is easily specified. This is shown to be the convex hull of the material set, and is thus named the *material hull*. Each point in the material hull represents a distinctive microstructure. Consideration of the material hull in design has the great advantage that all microstructures can be considered simultaneously, and thus microstructure becomes a design variable.

The class of microstructure–properties relationships that are of interest to MSD is presently that class associated with an intermediate scale of microstructure representation. This *mesoscale* representation includes the spatial distribution of crystallite phase and orientation in the microstructure; it follows that it includes grain size and shape, phase and orientation distribution and spatial correlations of these; and it also includes the first-order description of defect structure. Examples of the latter include the geometrically necessary dislocation density tensor (Sun et al., 2000) and the grain boundary character distribution (Watanabe, 1984). In the case study presented in this paper, elementary microstructure–properties relationships are used for initial yielding and elastic stiffness. Extension of MSD to more complex relationships requires material sets and hulls of higher dimension; the nature of these extensions is described in Section 4, but not fully developed. The most important problems in design tend to place demands on both defect-insensitive and defect-sensitive properties of materials; the latter (e.g., stress corrosion cracking, embrittlement, etc.) require spectral representations that

describe the spatial correlation of phase and orientation in the microstructure, and thus they demand more complex material sets and hulls.

It is demonstrated that the salient microstructure–properties relationships will often take the form of a family of surfaces (often hyperplanes) in the Fourier space. These are called *iso-property surfaces*, given the fact that all microstructures lying on any particular iso-property surface are predicted to have identical properties. Whenever an iso-property surface intersects the material hull, the intersection set represents microstructures (and their concomitant properties) that occur in natural materials. Details of the placement of the iso-property surface in the material hull impact the predicted properties. For example, extremal points of intersection of the iso-property planes represent the limiting values of properties that can be achieved by alterations of the microstructure. Another important feature of iso-property surfaces is that they typically reside in finite-dimensional subspaces of the full spectral representation. The implication is that all microstructures associated with identical projections into the residence subspace of the relevant iso-property surface have the same predicted properties.

The central tenets of MSD will be demonstrated by consideration of the design of a compliant fixed-guided beam. Compliant beams are important components in many compliant mechanisms (cf. Midha et al., 1994). The reader should note that the mechanical framework for this case study was deliberately selected to simplify the problem as much as possible for pedagogical clarity. We focus on the process whereby design objectives and constraints are communicated in the language of the Fourier space, rather than on the mechanics of the beam. Within the selected mechanical framework, the relevant microstructures are shown to belong to the class of axis-distribution functions. It is demonstrated that for this case study the main design objective and two constraints are readily communicated as two iso-property planes. Furthermore, it is found that optimization requires a compromise location for both planes, a compromise that stipulates a family of microstructures that are distinctly poly-axial (rather than single-axial) in nature.

Following the description of the case study, brief mention is made of directions for extending these elementary considerations to more advanced microstructure–property relationships, and to highly constrained design problems where defect-insensitive and defect-sensitive material properties may both be important.

3. Case study: MSD for a compliant beam

Consider design of a compliant fixed-guided beam as a prototypical component in this setting. Compliant beams are essential components of many compliant mechanisms (Midha et al., 1994). Fig. 1 is a schematic of the beam, which describes its function under fixed-guided (parallel) displacement of its ends.

3.1. Stipulation of design objectives and constraints

The *primary objective* in the compliant beam is minimization of the length of the beam, L, at specified deflection, Q. The beam must provide this deflection without

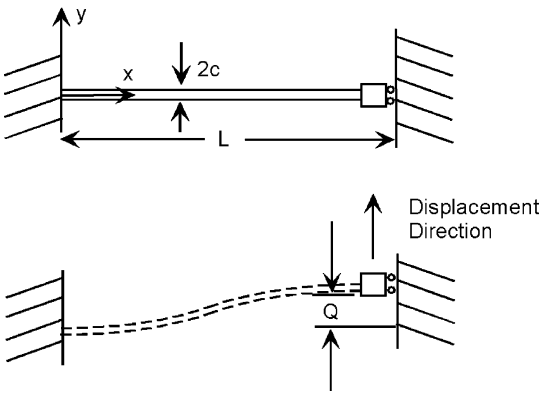

Fig. 1. Schematic of the compliant fixed-guided beam.

plastic yielding (*primary constraint*). Thus, both elastic and yielding properties are germane to the problem. A *secondary constraint* is that the beam must supply adequate restoring force to perform its function in the mechanism, without excessive beam width.

3.2. Mechanical framework

We choose to consider the mechanics of the beam using elementary plane-strain Bernoulli–Euler beam theory (cf. Juvinall, 1967). Within this framework, material planes that are initially perpendicular to the beam axis remain planes, perpendicular to the neutral axis of the beam upon deflection. The predicted strain field has only one non-zero component:

$$\varepsilon_{xx} = \alpha \left(\frac{Qy}{L^2} \right) \left(\frac{12x}{L} - 6 \right). \tag{1}$$

Here the index x refers to the x-axis of the beam as shown in Fig. 1, $\alpha = (1 + v)(1-2v)/(1-v)$ and v is Poisson's ratio. It is evident from (1) that concern for yielding is focused on the regions of highest strain near the surfaces $y = \pm c$ and corners $x = 0$, L. Hereafter the maximum strain value is denoted by ε:

$$\varepsilon = \frac{\alpha 6 Qc}{L^2}. \tag{2}$$

3.3. Evaluation of the compliant beam: traditional approach

The conventional approach to the compliant beam problem might proceed as follows. The beam is assumed to consist of a homogeneous material with isotropic elastic properties, which are specified by Young's modulus, E. Within the stated framework, the maximum levels for the non-zero stress components are given by

$$\sigma_{xx} = \left(\frac{E}{\alpha} \right) \varepsilon, \qquad \sigma_{yy} = \sigma_{zz} = \left(\frac{Ev}{\alpha(1-v)} \right) \varepsilon. \tag{3}$$

If the von-Mises yield criterion is selected to evaluate the primary constraint, the following expression is obtained:

$$\left(\frac{E}{1+\nu}\right)\varepsilon \leqslant \sigma_y. \tag{4}$$

It follows that optimizing the performance of the beam, in terms of the primary objective and primary constraint (which is tantamount to maximizing ε without yielding the material), requires selection of material with the largest possible ratio of $(1+\nu)\sigma_y/E$. (This is almost the same as maximizing σ_y/E, given the much larger variation of E among the candidate materials, as compared to variations in ν. Hereafter the effects due to variation in ν are neglected.)

In order to meet the requirements of the secondary constraint, we note that the restoring force is linearly dependent upon E/α. Neglecting the small effect from α, it follows that sufficient restoring force, without excessive beam width, requires that $E \geqslant E^*$ where E^* is to be determined by the specific application for the beam and its allowable width.

Evidently, this secondary constraint limits the reduction of E that tends to improve the performance of the primary beam relative to the primary objective and constraint of the design. Conventional design methodology then considers candidate materials, evaluating the ratio σ_y/E for each candidate material, subject to the constraint $E \geqslant E^*$. Material is often selected on this basis. There is usually neither an explicit consideration of microstructure nor an attempt to benefit from potential sources of anisotropy in the available materials.

An "enlightened" design team may consider potential sources of anisotropy, and improvements in performance that might be obtained from them. For example, if cubic metal alloys are of primary interest, the design team may recognize that a preferential alignment of $\langle 1\,0\,0\rangle$ crystal directions with the x-direction of the beam would tend to minimize E in that direction in some cubic materials. However, consideration of yielding would lead to the conclusion that the initial yield strength would tend to be increased by a preferential alignment of $\langle 1\,1\,0\rangle$ or $\langle 1\,1\,1\rangle$ crystal directions with the x-direction of the beam.[1] Obviously, the two kinds of preferred axial-distributions suggested by these elementary considerations are contrary to one another. A rigorous analysis using available crystal mechanics would suggest a particular axial distribution that maximizes the ratio σ_y/E, but then the analysis only considers uni-axial distributions, and not poly-axial ones. As shown later, a full consideration of crystal mechanics for the present problem leads to the conclusion that poly-axial distributions are optimal for the design of the compliant beam, rather than the uni-axial ones.

[1] Microstructures that consist of grains with one crystallographic axis fixed with respect to a specified macroscopic direction are hereafter called "axial-distributions", or "uni-axial distributions". The reader should note that, for such, information about the distribution of crystallographic axes that lie off the specified axis is not relevant.

3.4. Crystal mechanics

We shall assume that relation (1) describes the strain in the beam to an adequate approximation, at both the macroscopic level and at the grain level. This is consistent with the well-known uniform-strain assumption that leads to an upper-bound on the stored elastic energy in the beam (Hill, 1952; Paul, 1960). It follows that the stress field in the beam varies spatially according to Hooke's law,[2] applied at the local level:

$$\sigma_{ij} = C_{ijxx}\varepsilon_{xx}. \tag{5}$$

C, the elastic stiffness tensor, is a function of the phase and orientation of the local crystallite at the point of evaluation.

At this juncture we shall assume that the microstructure of the beam consists of a single-phase cubic material. Consideration of the symmetry of the cubic crystal shows that the local elastic stiffness tensor has the form

$$C_{ijkl} = C^o_{12}\delta_{ij}\delta_{kl} + C^o_{44}(\delta_{ik}\delta_{jl} + \delta_{il}\delta_{jk}) + (C^o_{11} - C^o_{12} - 2C^o_{44})g_{ir}g_{jr}g_{kr}g_{lr}, \tag{6}$$

where C^o_{11}, C^o_{12}, C^o_{44} are the three independent elastic constants for the reference cubic crystal (cf. Hirth and Lothe, 1968), and g_{ij} are components of the second-order rotation tensor that transforms the reference crystal[3] to coincide with the local crystallite characteristic of the neighborhood of the specified local position.

The question of yielding is formulated in a particular way that utilizes the uniform strain-rate upper-bound condition in crystal plasticity, as described by Hutchinson (1976). In particular, the overall rate of plastic working, $\dot{W}^{\mathrm{p}}$, is bounded above by the volume average of the local rates of plastic working, according to the expression

$$\dot{W}^{\mathrm{p}} \leqslant \langle \dot{w}^{\mathrm{p}} \rangle = \langle \sigma_{ij}\dot{\varepsilon}^{\mathrm{p}}_{ij} \rangle. \tag{7}$$

In relation (7) the angular brackets, $\langle \cdots \rangle$, denote volume averaging, $\dot{\varepsilon}^{\mathrm{p}}_{ij}$ is the local plastic strain rate, and $\dot{w}^{\mathrm{p}}$ is the local rate of plastic working. Initial yielding is taken to occur when $\dot{W}^{\mathrm{p}}$ just reaches a minimum observable level, $\dot{W}^{\mathrm{p}} = \dot{W}^{\mathrm{P}}_{\mathrm{obs}}$. Stress states for which the predicted rate of plastic working is lower than $\dot{W}^{\mathrm{P}}_{\mathrm{obs}}$ are defined to lie within the elastic limit. Following Hutchinson, the local constitutive law is taken to have a power-law dependence upon the resolved shear stress on each slip system, according to the expression

$$\frac{\dot{\gamma}^{(s)}}{\dot{\gamma}_o} = \left| \frac{\tau^{(s)}}{\tau^{(s)}_{\mathrm{c}}} \right|^n \mathrm{sign}(\tau^{(s)}), \tag{8}$$

where $\dot{\gamma}^{(s)}$ denotes the slip rate on slip system (s), $\tau^{(s)}$ and $\tau^{(s)}_{\mathrm{c}}$ denote the resolved shear stress and the reference value of slip resistance of slip system (s), respectively;

[2] In this paper repeated indices imply summation over the integers 1,2,3 according to the Einstein summation convention, except as otherwise noted. In relation (5), no summation is implied by the repeated x index.

[3] The reference crystal is taken to be oriented such that its basis vectors are of fixed relationship to a chosen external reference frame. For the cubic phases considered here the $\langle 1\,0\,0 \rangle$ crystal directions are taken to be parallel to the orthonormal external reference frame.

$\dot{\gamma}_o$ is a reference slip rate, and n is the power-law exponent (inverse rate sensitivity parameter). The resolved shear stress on slip system (s) is related to the Cauchy stress by the expression

$$\tau^{(s)} = \mu_{ij}^{(s)} \sigma_{ij}. \tag{9}$$

The geometrical aspects of this expression are contained in the slip tensors, $\mu^{(s)}$, which are defined by

$$\mu_{ij}^{(s)} = \tfrac{1}{2}(m_i^{(s)} n_j^{(s)} + m_j^{(s)} n_i^{(s)}), \tag{10}$$

where $m^{(s)}$ and $n^{(s)}$ denote the unit slip vectors in the slip direction and slip-plane, respectively. The local plastic strain rate is then given by the sum over all potential slip systems according to

$$\dot{\varepsilon}_{ij}^{\mathrm{p}} = \sum_{(s)} \mu_{ij}^{(s)} \dot{\gamma}^{(s)}. \tag{11}$$

Assuming that the local stress state differs only negligibly from the elastic state at the onset of yielding, a maximum local rate of plastic work is obtained by combining relations (2), (5), (6), (8), (9) and (11):

$$\dot{w}^{\mathrm{p}} = \left[\frac{\dot{\gamma}_o (2C_{44}^o \varepsilon)^{n+1}}{(\tau_{\mathrm{c}})^n}\right] \left[\sum_{(s)} |(g_{xi} g_{xj} \mu_{ij}^{o(s)} + A g_{xr}^2 \mu_{rr}^{o(s)})|^{n+1}\right]. \tag{12}$$

Here $\mu^{o(s)}$ are the slip tensors in the reference crystal, and the reference value of slip resistance on each slip system is taken to be the same. Summation over indices i, j and r, but not x, is implied in relation (12). A is an anisotropy factor of the form

$$A = \frac{C_{11}^o - C_{12}^o - 2C_{44}^o}{2C_{44}^o}. \tag{13}$$

Note that the crystallite orientation dependence of $\dot{w}^{\mathrm{p}}$ is described in Eq. (12) in terms of components of the (active) rotation tensor g, which is taken to transform the reference crystal into the local one. Within the chosen mechanical framework and the assumptions taken, the local rate of plastic working depends only upon components of the form g_{xj}, where the index x refers to the x-direction in the beam (Fig. 1). More precisely, if spherical polar angles ϕ, β define the orientation of the x-direction of the beam, relative to the crystallographic basis $\langle 1\,0\,0\rangle$, then the following relations define g_{xj}:

$$g_{x1} = \sin\phi \cos\beta, \quad g_{x2} = \sin\phi \sin\beta, \quad g_{x3} = \cos\phi. \tag{14}$$

3.5. The fundamental zone and fourier representation of the local rate of plastic working

$\dot{w}^{\mathrm{p}}$ possesses the symmetry of the crystal lattice plus a center of inversion; thus the symmetry subgroup applicable to the problem is $G = O_h$. It follows that the range of

interesting spherical-polar angles lies in the asymmetrical unit triangle defined by the set of angle pairs Θ:

$$\Theta = \{(\phi, \beta) \,|\, 0 \leqslant \beta \leqslant \pi/4, \cot^{-1}(\sin\beta) \leqslant \phi \leqslant \pi/2\}. \tag{15}$$

Θ is the "fundamental zone" that is appropriate for the selected mechanical framework. (In mathematical terms, Θ is also identified with S^2/O_h, which is the (homogeneous) orbit space of right O_h cosets of S^2, formally defined as

$$\Theta \equiv S^2/O_h = \{\{h\gamma_1, \ldots, h\gamma_{N_G}\} \,|\, h \in S^2; \gamma_i \in O_h\}. \tag{16}$$

Here N_G is the order of the symmetry subgroup O_h, which is 48. Further details on the group-theoretical structure of this and other homogeneous spaces can be found in Brocker and tom Dieck (1985).)

The local (maximum) rate of plastic working, expressed in Eq. (12), is an example of a function of the form $f : \Theta \to \Re$, where $\Re$ denotes the real numbers. A complete set of orthonormal basis functions is available for Θ; they are known as the cubic symmetric surface spherical harmonics. These functions shall be given the symbol $\dot{k}_l^\mu(y)$, consistent with the notation of Bunge (1982). Here y denotes the unit vector whose components $y = (g_{x1}, g_{x2}, g_{x3})$ specify the location of the beam axis relative to the $\langle 1\,0\,0\rangle$ directions in the cubic crystal. Their relation to ϕ, β is given in (14). Any well-behaved function of the form $f : \Theta \to \Re$ can thus be expressed as a series of the form

$$f(y) = \sum_{l=0,4}^{\infty} \sum_{\mu=1}^{M(l)} F_l^\mu \dot{k}_l^\mu(y), \tag{17}$$

where $M(l)$ enumerates the cubic symmetric subspaces associated with the primary index, l (cf. Bunge, 1982). The $\dot{k}_l^\mu(y)$ functions satisfy the orthogonality relationship[4]

$$\oiint_\Theta \dot{k}_l^\mu(y) \dot{k}_{l'}^{\mu'}(y)\, \mathrm{d}y = \delta_{ll'}\delta\mu\mu'. \tag{18}$$

It is remarkable that the expression for the local (maximum) rate of plastic working, Eq. (12), contains powers of the components of y limited by the power-law exponent to $l = 2(n+1)$. It follows that the spectral representation of relation (12) is

$$\frac{\dot{w}^{\mathrm{p}}(y)}{K} = \sum_{l=0,4}^{2(n+1)} \sum_{\mu=1}^{M(l)} P_l^\mu \dot{k}_l^\mu(y), \tag{19}$$

where K is $\dot{\gamma}_o(2C_{44}^o\varepsilon)^{n+1}/\tau_{\mathrm{c}}^n$, and the coefficients of the series expansion have been named P_l^μ to remind us that we are dealing with a property of the material. Only even l will appear in relation (19) owing to the centro-symmetry of the rate of plastic working; i.e., $\dot{w}^{\mathrm{p}}(y) = \dot{w}^{\mathrm{p}}(-y)$.

[4] Normally, orthogonality relations like the one shown in Eq. (18) would be expressed in terms of a complex conjugate of the primed basis function. Here, however, the cubic symmetry of the basis functions dictates that they are real.

3.6. Definition of the material set and material hull

Return next to consideration of the primary objective and constraint in connection with relation (7). The macroscopic (maximum) rate of plastic working is bounded from above by the volume average of the local (maximum) rate of plastic working, according to relations (7) and (12). For statistically homogeneous microstructures the volume fraction of grains that are oriented such that the x-axis of the beam is aligned with direction y (relative to the crystal basis) can be expressed by an axis distribution function $A(y)$ (cf. Bunge, 1982):

$$\frac{\mathrm{d}V}{V} = A(y)\,\mathrm{d}y. \tag{20}$$

The function $A(y)$ is readily expressed as a Fourier series of the form described in relation (17), but here we will take a different approach.

Let us consider uni-axial distribution functions of a dirac-delta character. For example, suppose that the axial distribution has only grains with orientation y_j relative to the crystal basis. Thus, we define a particular uni-axial distribution, $\delta(y - y_j)$, according to the conventional recipe:

$$\iint_{\Omega} \delta(y - y_j)\,\mathrm{d}y = \begin{cases} 1 \text{ if } y_j \in \Omega, \\ 0 \text{ if } y_j \notin \Omega, \end{cases} \tag{21}$$

where $\Omega \subset \Theta$. These dirac functions can be expressed in a series of the form

$$\delta(y - y_j) = \sum_{l=0,4}^{\infty} \sum_{\mu=1}^{M(l)} \dot{k}_l^{\mu}(y_j)\dot{k}_l^{\mu}(y). \tag{22}$$

Thus, the coefficients for the dirac distributions are just the cubic symmetric surface spherical harmonics, themselves, evaluated at y_j.

It is now a straightforward matter to specify the material set, which is just the fundamental zone, but expressed in the Fourier space. We shall use M_{c} as the symbol for this set. Note that M_{c} is an isomorphism of Θ. Let p denote a point in the Fourier space. The coordinates of p are the coefficients of the series expansion F_l^{μ}. The infinite set $\{F_l^{\mu}\}$ is synonymous with point p. Based upon Eq. (22) it is evident that the *material set*, M_{c}, is described as the set

$$M_{\mathrm{c}} = \{\, p \mid p = \{F_l^{\mu}\}, F_l^{\mu} = \dot{k}_l^{\mu}(\phi, \beta), (\phi, \beta) \in \Theta \}. \tag{23}$$

Fig. 2 shows the material set for the pertinent axis distribution function in the three-dimensional subspace with coordinates of the type (F_4^1, F_6^1, F_8^1). Given that M_{c} depends only upon two independent variables, it is evident that it has the form of a surface in any three-dimensional subspace.

Now consider the class of microstructure representations that are poly-axial distributions, $A(y)$; these can be formed by summing together an arbitrary number of uni-axial distributions. If v_j denotes the volume fraction associated with Dirac distribution $\delta(y - y_j)$, then the distributions of interest are described by

$$A(y) = \sum_j v_j \delta(y - y_j) = \sum_j \sum_{l=0,4}^{\infty} \sum_{\mu=1}^{M(l)} v_j \dot{k}_l^{\mu}(y_j)\dot{k}_l^{\mu}(y) \quad \left(\sum_j v_j = 1 \right). \tag{24}$$

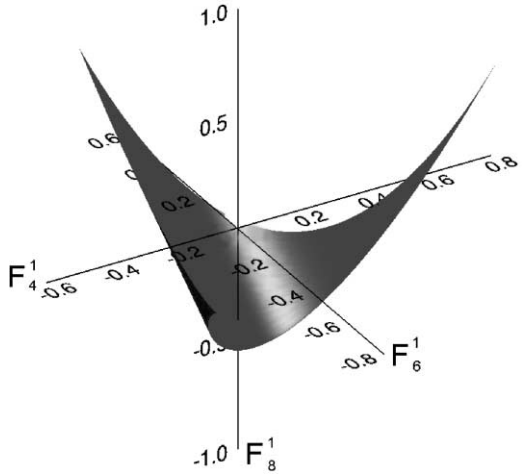

Fig. 2. Depiction of the material set M_c in a three-dimensional subspace.

As a practical matter, all axial distribution functions of interest can be deconstructed in the form suggested by relation (24). Note that the relevant coefficients for the distribution are just

$$F_l^{\mu} = \sum_j v_j \dot{k}_l^{\mu}(y_j) \tag{25}$$

(If a continuous description of volume fraction is preferred, it can be introduced via Eq. (20) by replacing the finite set of v_j weighting factors with $A(y)\,\mathrm{d}y$.)

We are now in a position to define the material hull comprising all possible microstructures of relevance to the compliant beam problem (within the context of Bernoulli–Euler mechanics and the other assumptions taken in formulating the problem). Expression (25) suggests that by considering the set of all possible sets of Fourier points $\{p_j\}$ ($p_j \in M_c$),[5] and corresponding weighting factors $\{v_j\}$, subject to the constraint that these must sum to one, then all possible axis distributions will have been considered. But this is just the convex hull of the material set. *Thus, the material hull M, representing all possible microstructures, is the convex hull of the material set M_c as defined by the expression*

$$M = \left\{ p \mid p = \sum_j v_j p_j, \{p_j\} \in \wp M_c, \{v_j\} \in \aleph \right\}. \tag{26}$$

Here the set $\aleph$ is formally defined to be a particular subset of the power set of X, $\aleph \subset \wp X$, where X is the set of real numbers that lie in the interval $[0,1]$, and all elements of $\aleph$ must be sets (of weighting factors) that, when summed over their elements,

[5] Any such set belongs to the power set of M_c, or $\wp M_c$.

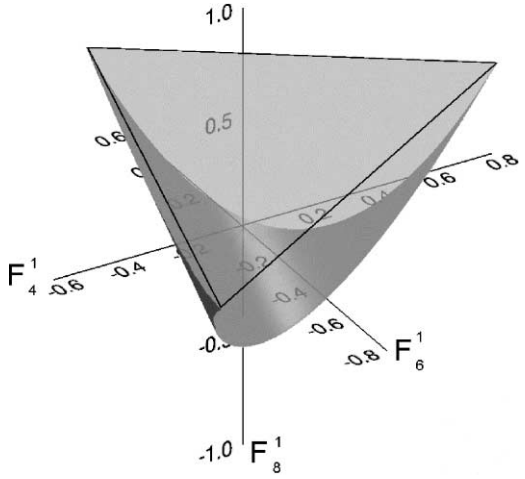

Fig. 3. Depiction of the material hull M in a three-dimensional subspace.

equal one. Thus,

$$\aleph = \left\{ \{v_j\} \,|\, \{v_j\} \in \wp X, X = [0,1], \sum_j v_j = 1 \right\}. \tag{27}$$

In simple words, the material hull is comprised of any combination of (physically distinctive) axial distributions (of the x-axis of the beam), weighted by volume fractions that sum to one.

Fig. 3 depicts the material hull M of all possible axial distributions pertinent to the compliant beam problem. As in Fig. 2, only the three-dimensional projection is shown. It is known that orthogonal projections of convex hulls into any subspace remain convex (Rockafellar, 1970). Thus, Fig. 3 is just the convex hull of Fig. 2. Note that the material hull includes the material set: $M_c \subset M$ according to relations (26) and (27).

3.7. The iso-property surfaces

We note that in statistically homogeneous microstructures, the bounding relation (7) is equivalent to

$$\dot{W}^p \leqslant \oiint_\Theta A(y)\dot{w}^p(y)\,\mathrm{d}y. \tag{28}$$

Expressing $A(y)$ as a series of cubic symmetric surface spherical harmonics, it follows from relations (18) and (19) that

$$\frac{\dot{W}^p}{K} \leqslant \sum_{l=0,4}^{2(n+1)M(l)} \sum_{\mu=1} F_l^\mu P_l^\mu. \tag{29}$$

Eq. (29) defines a closed half-space in on a finite subspace of the full spectral representation. The dimension of the pertinent subspace is determined by the maximum size of index l, which is $2(n+1)$.

For the purposes of interest here, the focus is upon the bounding plane of the closed half-space, which is defined by the equation

$$\frac{\dot{W}^{\mathrm{p}}}{K} = \sum_{l=0,4}^{2(n+1)} \sum_{\mu=1}^{M(l)} F_l^{\mu} P_l^{\mu}. \tag{30}$$

Given that the zeroth-order coefficient of the axial distribution, F_0^1, is a constant that is independent of the distribution itself, we prefer to rewrite Eq. (30) in the following form:

$$K' = \frac{\dot{W}^{\mathrm{p}}_{\mathrm{obs}}}{K} - F_0^1 P_0^1 = \sum_{l=4}^{2(n+1)M(l)} \sum_{\mu=1} F_l^{\mu} P_l^{\mu}, \tag{31}$$

where we have also set $\dot{W}^{\mathrm{p}} = \dot{W}^{\mathrm{p}}_{\mathrm{obs}}$, which defines the onset of yielding in the material as described earlier. *Relation* (31), *the bounding hyperplane in Fourier space*, *is the pertinent iso-property plane associated with the primary objective and primary constraint of the compliant beam design*. The normal to the plane is described by the coefficients $\{P_4^1, P_6^1, \ldots, P_{2(n+1)}^{\max \mathrm{M}(2(n+1))}\}$. Note that these are dependent upon constants of the reference crystal and the form of the chosen constitutive relations. All physically realizable sets of coefficients, with low-order coefficients $\{F_4^1, F_6^1, \ldots, F_{2(n+1)}^{\max \mathrm{M}(2(n+1))}\}$ selected such that relation (31) is satisfied, are predicted to achieve the performance described by the constant K'. Hence the terminology, "iso-property surface".

It is not difficult to show that the secondary constraint on restoring force is also described by a set of iso-property surfaces of the form

$$K'' = E^* - \frac{Q_0^1}{\sqrt{4\pi}} = F_4^1 Q_4^1, \tag{32}$$

where $Q_0^1 = 1.418(C_{12}^o + 2C_{44}^o) + 2.128C_{44}^o$ and $Q_4^1 = 1.240AC_{44}^o$. Relation (32) is a hyperplane perpendicular to the F_4^1 coordinate axis in the Fourier space; its position is entirely fixed by the elastic constants of the cubic phase, and by E^*.

3.8. Selection of optimal microstructures for the compliant beam

Relations (31) and (32) define the salient iso-property hyperplanes for the compliant beam. In the case of the primary objective and constraint, embodied in Eq. (31), a range of performances are predicted based upon where the iso-property hyperplane intersects the material hull. This range is illustrated for Ni-based alloys in Fig. 4. Note that the two hyperplanes identified are simple translations, one of the other, parallel to the plane normal. Hyperplane normals are defined by the P_l^{μ} coefficients for the particular cubic phase of interest. Table 1 lists these coefficients for several cubic phases, for a power-law exponent of $n = 15$.

Peak performance of the beam is realized when K' is minimized; this is equivalent to maximizing the ratio of Q/L, or minimizing L for fixed Q. This occurs for microstructures where the intersection of the iso-property hyperplane with the F_4^1 coordinate is

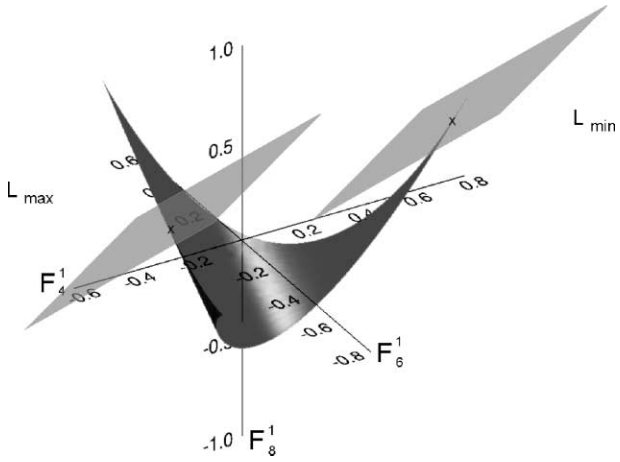

Fig. 4. Extremal positions for the primary iso-property hyperplane for Ni-based alloys. (Although difficult to visualize, the left extremal plane position intersects the material set, and material hull, at a single (marked) point. This point of intersection is the $\sim\langle 7\,7\,3\rangle$ axial distribution. See Table 2.)

maximized in the case of Ni-, Fe- and Cu-based alloys, and minimized in the case of W-, Mo- and Al-based alloys. The associated range of predicted performance associated with the primary iso-property hyperplanes is recorded in Table 2, along with their associated axial-distributions.

Consideration of the secondary constraint, embodied in Eq. (32) leads to the conclusion that the sign of anisotropy ratio A (see Eq. (13)) determines the variation of restoring force with respect to coordinate F_4^1. Maximizing K'' maximizes the restoring force (at fixed beam width), and since A is negative for Al-, Ni-, Fe- and Cu-based alloys, reducing F_4^1 is required to increase the restoring force. For Mo-based alloys the opposite is true, and for W-alloys the restoring force is insensitive to coordinate F_4^1, or any other aspect of microstructure within the framework we have selected. Table 3 lists the Q_0^1 and Q_4^1 coefficients for the selected cubic phases.

Note that physically-possible solutions occur only when these iso-property hyperplanes have non-empty intersection with each other, and with the material hull (described by relations (23), (26) and (27)). The relevant solution set is just the set of all microstructures described by this intersection.

A particular solution set is illustrated in Fig. 5 for the case of Ni-based alloys. Given that the primary objective and constraint is optimized by pushing the coordinate F_4^1 to be as large as possible, while sufficient restoring force places a limit on how large F_4^1 is allowed to be, a particular compromise is shown in Fig. 5. The gray plane represents the iso-property plane for the primary objective and constraint, while the brown plane represents performance in restoring force (secondary constraint). F_4^1 has been shifted some distance off of the maximum allowable value in order to provide for the secondary constraint. The intersection of the two hyperplanes falls within the material hull, but clearly not on the material set. This is highlighted as a yellow line

Table 1
List of iso-property hyperplane coefficients, P_l^{μ} , for relation (32) for selected cubic phases

l	μ	Al	Fe	Mo	Cu	Si	W	Ni
0	1	1.12E − 06	1.42E − 08	1.47E − 04	4.91E − 09	1.41E − 07	7.79E − 06	1.07E − 08
4	1	9.69E − 07	−2.91E − 08	4.74E − 04	−1.38E − 08	−6.22E − 08	1.50E − 05	−2.41E − 08
6	1	1.72E − 06	1.18E − 08	2.24E − 05	−1.89E − 09	2.45E − 07	8.04E − 06	6.19E − 09
8	1	−9.76E − 07	9.29E − 09	−3.03E − 05	5.16E − 09	−5.51E − 08	−6.57E − 06	8.36E − 09
10	1	1.19E − 06	−1.06E − 08	1.98E − 04	−3.64E − 09	3.42E − 08	1.11E − 05	−8.58E − 09
12	1	8.04E − 07	−2.94E − 10	4.49E − 05	−1.81E − 09	9.19E − 08	4.21E − 06	−1.36E − 09
12	2	−8.90E − 07	−2.19E − 08	−1.17E − 04	−8.47E − 09	−1.33E − 07	−6.33E − 06	−1.74E − 08
14	1	−1.33E − 07	−6.83E − 09	7.62E − 05	−1.62E − 09	−6.04E − 08	1.59E − 06	−4.88E − 09
16	1	8.18E − 08	−1.50E − 09	4.44E − 05	1.70E − 10	−1.74E − 08	1.72E − 06	−7.81E − 10
16	2	−2.79E − 07	−8.08E − 11	−4.47E − 05	1.60E − 09	−3.67E − 08	−1.99E − 06	7.54E − 10
18	1	−1.28E − 07	6.22E − 10	7.17E − 06	6.03E − 10	−1.51E − 08	−4.45E − 07	7.43E − 10
18	2	2.64E − 08	−4.38E − 11	1.15E − 05	3.31E − 10	−1.12E − 09	3.71E − 07	1.08E − 10
20	1	−1.74E − 08	2.99E − 10	9.17E − 06	2.55E − 11	−1.26E − 09	8.83E − 08	2.10E − 10
20	2	−5.52E − 08	8.81E − 11	−9.37E − 06	−7.49E − 11	−4.54E − 09	−4.16E − 07	6.40E − 11
22	1	−1.11E − 08	−5.61E − 11	4.01E − 07	−1.06E − 10	−3.99E − 11	−7.61E − 08	−8.60E − 11
22	2	−2.20E − 08	1.31E − 10	9.18E − 07	6.34E − 11	−2.71E − 09	−7.47E − 08	1.33E − 10
24	1	5.59E − 10	−1.94E − 11	1.21E − 06	−7.41E − 12	1.90E − 10	1.26E − 08	−1.86E − 11
24	2	−2.23E − 08	−1.79E − 10	−2.18E − 06	−3.40E − 11	−2.70E − 09	−1.39E − 07	−1.23E − 10
24	3	2.66E − 08	5.52E − 10	7.32E − 07	1.62E − 10	4.83E − 09	1.14E − 07	4.07E − 10
26	1	−1.60E − 09	−1.76E − 11	3.67E − 08	6.50E − 12	−2.46E − 10	−8.53E − 09	−8.02E − 12
26	2	−1.93E − 09	4.91E − 11	−8.71E − 08	5.24E − 12	2.20E − 10	−1.79E − 08	3.21E − 11
28	1	1.16E − 10	−2.97E − 13	1.34E − 07	4.19E − 13	−2.58E − 12	2.24E − 09	1.01E − 13
28	2	−2.82E − 09	1.44E − 11	−3.92E − 07	6.74E − 12	−1.61E − 10	−2.28E − 08	1.28E − 11
28	3	2.95E − 09	−1.59E − 11	1.73E − 07	−1.48E − 11	2.82E − 10	1.74E − 08	−1.77E − 11
30	1	−1.34E − 10	8.86E − 13	−2.78E − 09	8.81E − 15	−1.03E − 11	−8.29E − 10	6.92E − 13
30	2	5.24E − 11	−1.11E − 12	−4.03E − 09	−5.57E − 13	1.87E − 11	−3.87E − 10	−1.13E − 12
30	3	−1.01E − 10	−6.87E − 13	−2.04E − 08	−6.59E − 13	2.41E − 12	−1.24E − 09	−7.84E − 13
32	1	5.36E − 12	1.27E − 14	7.36E − 09	4.12E − 16	2.48E − 14	1.24E − 10	1.07E − 14
32	2	−1.13E − 10	−2.03E − 13	−2.69E − 08	−2.94E − 13	−3.51E − 12	−1.23E − 09	−2.67E − 13
32	3	1.19E − 10	1.92E − 13	1.06E − 08	4.71E − 13	5.96E − 12	8.91E − 10	2.98E − 13

Table 2
Ratio of predicted maximum and minimum beam lengths and their associated axial-distributions for selected cubic phases ($\langle u\,v\,w\rangle_{\min}$ is the axial-distribution associated with $L_{\min}$ and $\langle u\,v\,w\rangle_{\max}$ is the axial-distribution associated with $L_{\max}$.)

	Al	Fe	Mo	Cu	Si	W	Ni
$L_{\max} - L_{\min}/L_{\min}$	0.218	0.323	0.431	0.507	0.146	0.300	0.361
$\langle u\,v\,w\rangle_{\max}$	⟨9 4 0⟩	⟨7 7 3⟩	⟨9 3 0⟩	⟨7 7 3⟩	⟨8 5 1⟩	⟨9 4 0⟩	⟨7 7 3⟩
$\langle u\,v\,w\rangle_{\min}$	⟨1 1 1⟩	⟨1 0 0⟩	⟨1 1 1⟩	⟨1 0 0⟩	⟨1 0 0⟩	⟨1 1 1⟩	⟨1 0 0⟩

Table 3
List of Q coefficients for relation (32) for selected cubic phases (units of 10^{11} dyn/cm^2)

	Al	Fe	Mo	Cu	Si	W	Ni
Q_0^1	39.800	104.035	154.041	74.433	66.897	184.747	108.707
Q_4^1	−0.626	−7.967	3.968	−6.436	−3.559	0.000	−9.312

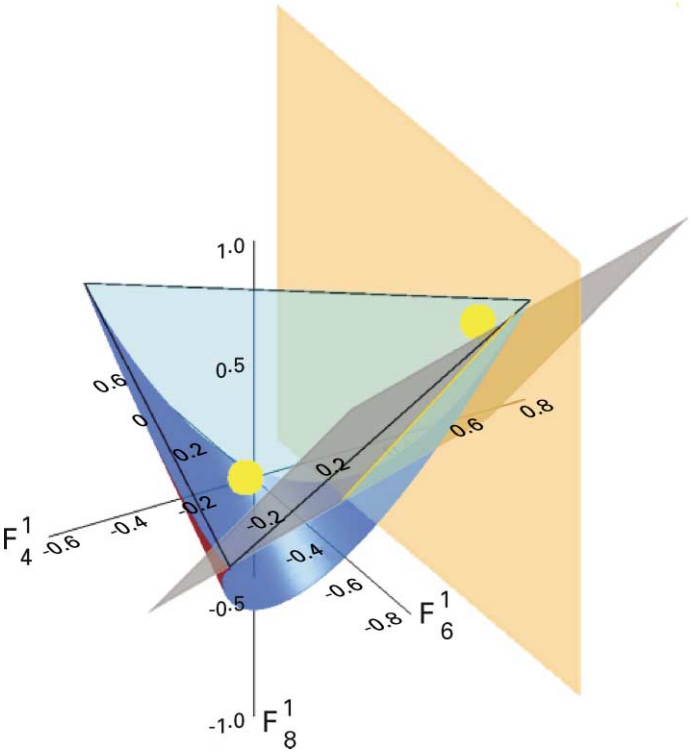

Fig. 5. Depiction of the optimal solution set (yellow line segment), formed by the intersection of iso-property planes for the primary objective and constraint (gray) and the secondary constraint (brown) with the material hull (blue). Yellow points indicate the microstructure of rolled Ni (left) and rolled+recrystallized Ni (right).

segment in Fig. 5. Note that all members of the set of optimal microstructures are poly-axial, rather than uni-axial.

3.9. Processing considerations

Next, consider the problem of guiding processing conditions to achieve a microstructure within the optimal set. An empirical approach is illustrated. The yellow points in Fig. 5 depict the locations in the Fourier subspace for two nickel-alloy microstructures that were characterized by the authors. The point to the left is for rolled nickel alloy, and the point to the right is for the same rolled nickel, but following a subsequent recrystallization anneal. Notably, the two microstructures lie on opposite sides of both selected iso-property planes. Transformation of the deformed microstructure, by annealing, can be represented as a streamline (not shown) connecting the deformed microstructure to the deformed + annealed microstructure. It is evident that this streamline must pass from left to right, cutting through the iso-property planes somewhere quite near the optimal set in the material hull (yellow line segment). Thus, we

conclude that deformation, followed by a partial recrystallization annealing treatment (to be determined) could result in a microstructure near the optimal set.

3.10. Summary of the case study

By way of summary, the application of MSD to the design of the compliant (fixed guided) beam demonstrates the following principles:

(a) Those aspects of microstructure that are important to any particular design problem are dictated by the mechanics and physics of the problem. (In the design of a compliant beam, only the distribution of orientations of the beam axis, with respect to the crystal basis, is found to be important.)
(b) Spectral representation of the relevant aspects of microstructure has the profound advantage that the entire universe of possible microstructures can be conveniently represented. (This is the material hull.)
(c) Design objectives and constraints are conveniently interpreted as families of iso-property surfaces in the same Fourier space. (These were found to be hyperplanes in the compliant beam problem. Two such planes were required to represent the design objective and two constraints in the case study.)
(d) The optimal set of microstructures for a design problem is defined by the intersection of the iso-property plane(s) with the material hull, with the position of those planes optimally located for design performance. (In the compliant beam, an optimal location was determined by a compromise between the competing objective and constraints of the problem.)
(e) Once the optimal set of microstructures has been identified, guidance for candidate processing paths is facilitated by empirical and theoretical considerations in the Fourier space. (A candidate processing path was identified for producing a near-optimal microstructure for the compliant beam.)
(f) Treatment of the entire design problem in the spectral representation facilitates a deeper level of communication between the designer and the materials engineer, opening up the design space to the consideration of material microstructure as a design variable, and pointing to solutions where microstructure has been optimized.

4. Extension of MSD to problems of higher dimension

For the case study just presented, MSD required only elementary volume fraction information on crystal orientation in the microstructure. Two limitations are encountered when solutions are restricted to volume fraction data. First, although the bounding aspect of the solution for the compliant beam was not emphasized, bounds on linear (defect-insensitive) properties, can be rather widely separated. Thus, predictions of upper- and lower-bounds on defect-insensitive properties (like the elastic stiffness, thermal conductivity, and initial yield-strength) can be too imprecise to be useful in solving highly constrained design problems. And second, even the most elementary of physical models for defect-sensitive properties, like intergranular stress corrosion cracking, require information about the grain boundary character distribution (GBCD) of the

microstructure. And it is known that the GBCD requires 2-point correlation statistics on orientation (and/or phase) in the microstructure (Adams and Olson, 1998).

Here we proceed with a brief description of the anticipated extensions required to carry MSD to a framework of higher dimension. Two objectives will be important: obtaining more precise bounds on linear properties, and extending MSD to include defect-sensitive properties. To be precise, we describe the extensions required when the physical framework of the problem requires the 2-point orientation correlation statistics. (We restrict our attention to single phase polycrystals, but note that the extension required for poly-phase materials is straightforward.)

4.1. Improved bounds on linear properties

Reductions in the separation of upper- and lower-bounds on linear properties are predicted from the variational principles developed by Hashin and Shtrikman (1962a,b). Theoretical developments of Zeller and Dederichs (1973), Kroner (1977) and Willemse and Caspers (1979) obtained expressions for bounds on tensors of second and fourth order, incorporating higher-dimensional representations of microstructure for polycrystalline materials. These results were recently reviewed, and examined in a consistent notation by Adams and Olson (1998). The first application of the higher-dimensional theories to predict elastic properties in orthotropic polycrystals was reported by Beran et al. (1996) and Mason and Adams (1999). These incorporated the 2-point orientation correlation statistics, and demonstrated that the upper- and lower-bounds were narrowed by a factor of $\sim$5 as compared to bounds that used only volume fraction data. Comparisons with measured elastic constants showed these bounds to be in agreement with experimental measurements. It is also evident that these narrower bounds are likely to be of much greater interest in highly constrained design applications.

Consider a convenient bounding relationship that incorporates both 1- and 2-point statistics (Adams and Olson, 1998):

$$C^* < (>) C^r + A_1 (A_1 + A_2)^{-1} A_1, \tag{33}$$

where C^* is the predicted effective elastic stiffness of the polycrystalline material. (The reader should note that relation (33) must be interpreted as bounding the stored elastic strain energy, rather than individual components of the effective elastic stiffness tensor itself.) C^r is a reference stiffness tensor defined such that

$$\delta C(x) = C(x) - C^r < (>) 0 \tag{34}$$

for all positions x in the body of material. The fourth order tensors appearing in relation (33) are defined by

$$A_1 \equiv \langle C \rangle - C^r, \tag{35}$$

where, as before, $\langle \cdots \rangle$ denotes volume or ensemble averaging, and by

$$A_2 \equiv \langle \delta C \Gamma^r \delta C \rangle. \tag{36}$$

Γ^r signifies a specific integral Green's function operator that depends upon C^r and the shape of the body. One-point statistics (volume fractions) are required in relation (35), and 2-point correlation statistics are required to evaluate relation (36).

For single-phase materials, the required 2-point orientation correlation statistics can be expressed in the Fourier space in the manner described by Adams et al. (1987):

$$f_2(g,g'\,|\,r)=\sum_{l}\sum_{\mu}\sum_{\eta}\sum_{\lambda}\sum_{\sigma}\sum_{\rho}F_{l\lambda}^{\mu\eta\sigma\rho}(r)\dot{\dot{T}}_{l}^{\mu\eta}(g)\dot{\dot{T}}_{\lambda}^{\sigma\rho}(g'). \tag{37}$$

$f_2(g,g'\,|\,r)$ expresses the probability density that a randomly placed test vector of character r will sample orientation g at its tail and orientation g' at its head. The functions $\dot{\dot{T}}_{l}^{\mu\eta}(g)$ and $\dot{\dot{T}}_{\lambda}^{\sigma\rho}(g')$ are crystal symmetric generalized spherical harmonic functions (cf. Bunge, 1982). $F_{l\lambda}^{\mu\eta\sigma\rho}(r)$ are the Fourier coefficients in the 2-point space. (That the basis for the 2-point OCFs can be conveniently expressed as a product of basis functions that are orthogonal over the individual components of its product space, is a classical result in mathematical physics (cf. Courant and Hilbert, 1937).)

These six-index Fourier coefficients can be incorporated into relation (36) and then (33) in order to obtain improved bounds on linear properties. Note that the relevant fundamental zone for the 2-point framework is the product of two homogeneous spaces:

$$\Theta=\mathrm{SO}(3)/G\times\mathrm{SO}(3)/G. \tag{38}$$

As noted in Sections 2 and 3, G in (38) denotes the symmetry subgroup of the relevant crystal phase or material property, whichever is of higher order. The material set for each vector r consists of all of the points described by the six-index coefficients associated with specified orientation correlation characteristics in the microstructure (i.e., specified g and g'). The material hull comprises linear combinations of these characteristics, weighted by number fractions that must sum to one. Although details are not given here, it is evident that the spectral representation of $f_2(g,g'\,|\,r)$, relation (37), can be incorporated into relation (36) and then into relation (33), in order to form a family of iso-property surfaces. These surfaces, representing bounds on the stored elastic strain energy, will no longer be hyperplanes, but more complex surfaces with curvature.

4.2. Application to defect-sensitive properties

The first-order description of dependence of defect-sensitive properties (e.g., intergranular stress corrosion cracking, embrittlement, etc.) on characteristics of the microstructure is known to be through the GBCD. GBCD refers to the distribution of characteristics of grain boundaries, as specified by identifying the grain orientation on each side of the boundary, say g and g', and the inclination of the boundary tangent plane, n. The GBCD is here named $S_V(g,n,g')$; it has units of surface area density of grain boundaries, per unit volume.

There exists a precise stereological connection between the 2-point statistics described in the previous section, and the GBCD (Adams et al., 1993):

$$\lim_{|r|\to 0}\left[\oiint_{s^2}S_V(g,n,g')|r\cdot n|\,\mathrm{d}n=f_2(g,g'\,|\,r)\right]. \tag{39}$$

It is convenient, in connection with the GBCD, to carry the inclination dependence of the distribution explicitly in the fundamental zone. Thus,

$$\Theta=\mathrm{SO}(3)/G\times S^2\times\mathrm{SO}(3)/G, \tag{40}$$

where S^2 is the set of directions that the inclination, n, can take. (It is convenient to think of S^2 as a unit sphere and its origin, with all vectors emanating from the origin to any point on the surface of the sphere representing possible inclinations, n.) The spectral representation of $S_V(g,n,g')$ is

$$S_V(g,n,g') = \sum_{l\mu n}\sum_{l'\mu' n'}\sum_{rs} S_{ll'r}^{\mu n\mu' n' s}\dot{\dot{T}}_l^{\mu n}(g)\dot{\dot{T}}_{l'}^{\mu' n'}(g')k_r^s(n). \tag{41}$$

(In this expression the $k_r^s(n)$ functions are surface spherical harmonics, but they are not symmetrized.) Corresponding to Eq. (41) are characteristic (dirac-like) density functions that have coefficients of the form

$$S_{ll'r}^{\mu n\mu' n' s} = \dot{\dot{T}}_l^{*\mu n}(g_j)\dot{\dot{T}}_{l'}^{*\mu' n'}(g'_j)k_r^{*s}(n_j), \tag{42}$$

where $*$ denotes complex conjugation. The relevant material set is just the set of sets of Fourier coefficients of the type given in (42), evaluated for all characteristics described in the fundamental zone (40). The material hull is then the convex hull of the material set, found by linear combinations of the elements of the material set, subject to their fractions equaling the total surface area, per unit volume, S_V, of grain boundaries in the polycrystal.

The eight parameter GBCD can be projected into lower-dimension subspaces by integration. For example, a five-parameter GBCD is defined by

$$\tilde{S}_V(\Delta g,n) = \iiint_{\mathrm{SO}(3)/G} S_V(g,n,g\cdot\Delta g)\,\mathrm{d}g, \tag{43}$$

where Δg is the misorientation between adjacent grains. Most of the work with GBCDs relates to the misorientation distribution function (MDF), $M(\Delta g)$, which is obtained by also averaging over the inclination dependence:

$$M(\Delta g) = \iint_{S^2}\iiint_{\mathrm{SO}(3)/G} S_V(g,n,g\cdot\Delta g)\,\mathrm{d}g\,\mathrm{d}n. \tag{44}$$

These reduced forms of the GBCD, $M(\Delta g)$ and $\tilde{S}_V(\Delta g,n)$, that have thus far been the focus of empirical correlations between grain boundary character and defect sensitive properties. These correlations have generally linked defect-sensitive properties to the fraction of occurrence of special classes of grain boundaries vicinal to coincidence site lattices (CSL). Examples include grain boundary segregation (Bouchet et al., 1988; Hofmann, 1990; Muschik et al., 1989; Powell and Woodruff, 1976; Watanabe et al., 1978; Yoshitomi et al., 1995), resistance to corrosion (Lin et al., 1995; Palumbo and Aust, 1995), stress corrosion cracking (Palumbo et al., 1991; Pan et al., 1996), and creep (Lehockey and Palumbo, 1997; Lehockey et al., 1997; Was et al., 1998). The application of these empirical correlations, in connection with various processing methods that achieve elevated levels of grain boundaries that are resistant to the various failure mechanisms, is called "grain boundary engineering" (Watanabe, 1984). It is known, for example, that repeated deformation (to intermediate strain levels) and annealing cycles can increase the occurrence of low energy boundaries in materials that twin easily (cf. Randle and Brown, 1989; King and Schwartz, 1998; Kumar et al., 2000).

To illustrate how these empirical correlations can be incorporated within MSD to consider design problems where defect sensitive properties are important, consider a

framework in which $\tilde{S}_V(\Delta g, n)$ is the important representation. This is a function with a series representation of the form

$$\tilde{S}_V(\Delta g, n) = \sum_{\lambda\mu\eta}\sum_{\sigma\xi} S_{\lambda\sigma}^{\mu\eta\xi}\,\ddot{\tilde{T}}_{\lambda}^{\mu\eta}(\Delta g)\dot{\tilde{k}}_{\sigma}^{\xi}(n). \tag{45}$$

As shown here, the misorientation dependence of the function is carried by the (doubly) crystal-symmetric generalized spherical harmonic functions, and the inclination dependence is described in the local crystal frame by the crystal symmetric surface spherical harmonic functions (Bunge, 1982; Adams and Olson, 1998). Next, assume that certain classes of grain boundary types have been identified as "good" in some sense (e.g., resistant to sensitization or stress corrosion cracking). Let these boundaries occupy specific subsets, $\Theta_j \subset \Theta$, of the fundamental zone, which for $\tilde{S}_V(\Delta g, n)$ is identified as

$$\Theta = G\backslash \mathrm{SO}(3)/G \times S^2/G. \tag{46}$$

The total surface area per unit volume of "good" boundaries, $\tilde{S}_V^{+}$, is thus found depend upon the microstructure according to the relation

$$\begin{aligned}\tilde{S}_V^{+} &= \sum_{\lambda\mu\eta}\sum_{\sigma\xi} S_{\lambda\sigma}^{\mu\eta\xi}\sum_{j}\oiiint_{\Theta_j}\oiint \ddot{\tilde{T}}_{\lambda}^{\mu\eta}(\Delta g)\dot{\tilde{k}}_{\sigma}^{\xi}(n)\,\mathrm{d}n\,\mathrm{d}\Delta g \\ &= \sum_{\lambda\mu\eta}\sum_{\sigma\xi} S_{\lambda\sigma}^{\mu\eta\xi} B_{\lambda\sigma}^{\mu\eta\xi}.\end{aligned} \tag{47}$$

In the spirit of the empiricism that has thus far been advanced, microstructures with desirable defect-sensitive properties are achieved when

$$\frac{\tilde{S}_V^{+}}{\tilde{S}_V} \geqslant p_{\mathrm{c}}, \tag{48}$$

where $\tilde{S}_V$ is the total surface area per unit volume of grain boundary in the material, and p_{c} is a suitable percolation threshold (cf. Wells et al., 1989; Gaudett and Scully, 1994). Relation (47) in connection with relation (48) constitutes an iso-property hyperplane within the empirical framework described.

4.3. Distance measures in the Fourier space

It is evident that the step to higher dimensionality is a demanding one, if only for the fact that the main representation of microstructure, the 2-point OCFs, have 6 independent variables (8 in the case of the full GBCD where the inclination dependence is also represented in the Fourier series). This is to be compared with 2 independent variables in the case study presented in Section 3. This higher dimensionality increases the complexity of visualizing the relevant sets in Fourier space using ordinary 3-D graphical methods. In order to proceed with MSD in this higher dimensional environment, it is necessary to rely upon metrics for distance in the Fourier space. For example, it may be necessary to express the distance between pairs of Fourier points (e.g., the distance between a microstructure, represented by a point in the Fourier space, and a second

point or collection of points lying upon a specified iso-property surface, or optimal set). A particular measure of distance is readily available, given that all of the representations of microstructure described in this paper (including $f_2(g,g'\,|\,r)$) belong to the class of square-integrable functions. It follows that a measure of (squared) distance between two microstructures, say $d^2(f_2,\bar{f}_2)\geqslant 0$, is defined by

$$d^2(f_2,\bar{f}_2)=\fint\!\!\!\fint\!\!\!\fint\fint\!\!\!\fint\!\!\!\fint\!\!\!\fint[f_2(g,g'\,|\,r)-\bar{f}_2(g,g'\,|\,r)]^2\,\mathrm{d}g\,\mathrm{d}g', \tag{49}$$

where the integration is over the entire range of all six variables. Expression of distance in terms of the Fourier coefficients follows by introducing series expansions of the form shown in Eq. (37) into the integrand, and then by applying the orthogonality relationships between the basis functions. The result is

$$\begin{aligned} d^2(f_2,\bar{f}_2)=&\sum_l\sum_m\sum_n\sum_\lambda\sum_\mu\sum_\eta\left(\frac{1}{2l+1}\right)\left(\frac{1}{2l+1}\right)\\ &\times[F_{l\lambda}^{mn\mu\eta}F_{l\lambda}^{*mn\mu\eta}-F_{l\lambda}^{mn\mu\eta}\bar{F}_{l\lambda}^{*mn\mu\eta}-\bar{F}_{l\lambda}^{mn\mu\eta}\bar{F}_{l\lambda}^{*mn\mu\eta}+\bar{F}_{l\lambda}^{mn\mu\eta}\bar{F}_{l\lambda}^{*mn\mu\eta}], \end{aligned} \tag{50}$$

where $*$ denotes the complex conjugate.

5. Summary

The main purpose of this paper is to demonstrate how design can be conducted such that information flow is facilitated in the opposite direction to the conventional approach, i.e. design objectives/contraints → material properties → microstructure → processing. This new paradigm, called microstructure sensitive design (MSD), has the advantage that the microstructure, and its concomitant properties, are considered to be continuous design variables.

The key to MSD is that all aspects of the problem are formulated with a spectral representation. When a particular physical framework is chosen to model constitutive behavior of the material, the dimensionality of the required Fourier space is determined.

Design objectives and constraints are conveniently communicated by specific iso-property surfaces in this space. In the case study presented, two iso-property surfaces were considered, and they both had the form of hyperplanes residing in a finite dimensional. Finite dimensionality is a typical characteristic of iso-property surfaces.

Microstructures are also represented by points in the Fourier space. Two aspects of microstructure representation were addressed. The complete set of components ("building blocks") from which the pertinent microstructures may be constructed was shown to occupy a compact set in the space, called the material set. Then, from the material set, we have shown how the universe of all microstructures pertinent to the mechanical framework of the design are points that reside in the convex hull of the material set. This convex hull was named the material hull. The material hull includes the material set as a subset. Both material set and material hull have infinite dimension in the Fourier space.

Intersections of the relevant (finite-dimensional) iso-property planes with the material hull (infinite-dimensional) identify sets of points that represent real physical microstruc-

tures that can be considered to meet design objectives/constraints. All points belonging to the intersection set are predicted to have the same performance with respect to the specific objective/constraint represented by the iso-property surface. When more than one iso-property plane is required by the design problem, then it is the reduced intersection of all such iso-property surfaces with the material hull that comprise the set of microstructures predicted to achieve the combined performance levels predicted by the several iso-property surfaces.

Optimal sets of microstructures for the specified design problem are found by translations of the pertinent iso-property surfaces to those limits that are dictated by the orientation and shape of the surfaces themselves. When the iso-property surfaces are hyperplanes, as they were in the case study, then translation of the hyperplane to extreme locations intersecting the material hull will maximize performance of the design with respect to the considered objective/constraint. For the case study, it was demonstrated that a $\langle 1\,0\,0\rangle$ uni-axial distribution of grain orientations was optimal for Ni, Fe, Cu and Si alloys when considering only the hyperplane representing the primary objective and constraint. ($\langle 1\,1\,1\rangle$ axial distributions were found to be optimal for Al, Mo and W.) However, a second hyperplane, representing the constraint of adequate restoring force, was shown to restrict the optimal class of microstructures to poly-axial distributions in the case of Ni.

MSD provides a framework for guiding the development of processing to achieve microstructures that lie near the optimal set. Much development remains to be done to properly connect MSD with existing models that describe the evolution of microstructure. Some work in this direction for deformation processing has been described by Bunge and Esling (1984). Extensions of this work to a wider scope of processing paths will be presented in a subsequent paper.

Extensions of MSD to highly constrained design problems is expected to demand material sets and hulls of higher dimension and complexity. Improved bounds on linear properties, and extensions to include defect-sensitive properties are both expected to require constitutive laws that incorporate characteristics of the spatial distribution of orientation (and/or phase) in the microstructure. Elementary treatment of this additional complexity requires microstructure representation by the 2-point orientation (and/or phase) correlation functions. Section 4 provides a roadmap that anticipates these extensions.

There appear to be many advantages of MSD to the design team. We anticipate that MSD enables efficient communication between the designer and the materials specialist, speeds up the design process, allows a much more complete consideration of a rich family of materials and microstructures, saves time and effort, and results in superior design solutions.

Acknowledgements

BA acknowledges financial support provided by the MRSEC Program of the National Science Foundation under Award Number DMR-9632556. SK acknowledges financial support from National Science Foundation under Award Number CMS-9732699. BA,

SK and HG also acknowledge support from the NSF-CIRE program centered at Florida A&M University, facilitating collaborations. Support was also provided by the College of Engineering and Technology at BYU (AH, BH and ML). Computations were performed on the new SGI Origin 2000 supercomputer at Brigham Young University, donated by Ira Fulton.

References

Adams, B.L., Morris, P.R., Wang, T.T., Willden, K.S., Wright, S.I., 1987. Description of orientation coherence in polycrystalline materials. Acta Metall. 35, 2935–2946.

Adams, B.L., Wright, S.I., Kunze, K., 1993. Orientation imaging: the emergence of a new microscopy. Metall. Trans. 24A, 819–831.

Adams, B.L., Olson, T., 1998. The mesostructure-properties linkage in polycrystals. J. Prog. Mater. Sci. 43, 1–88.

Bhattacharya, K., James, R.D., 1999. A theory of thin films of martensitic materials with applications to microactuators. J. Mech. Phys. Solids 47, 531–576.

Beran, M.J., Mason, T.A., Adams, B.L., Olson, T., 1996. Bounding elastic constants of an orthotropic polycrystal from measurements of the microstructure. J. Mech. Phys. Solids 44, 1543–1563.

Bouchet, D., Aufray, B., Priester, L., 1988. Experimental evidence of sulfur effect on the plane and on the extrinsic dislocations of a $\Sigma = 3$ grain boundary in nickel. J. Phys. 49, C5-417–C5-422.

Brocker, T., tom Dieck, T., 1985. Representations of Compact Lie Groups. Springer, New York, pp. 30–32.

Bunge, H.-J., 1965. Zur Darstellung allgemeiner Texturen. Z. Metallkde 56, 872–874.

Bunge, H.-J., 1982. Texture Analysis in Materials Science. Butterworths, London.

Bunge, H.-J., Esling, C., 1984. Texture development by plastic deformation. Scripta Metall. 18, 191–195.

Cherkaev, A., 2000. Variational Methods for Structural Optimization. Springer, New York.

Courant, R., Hilbert, D., 1937. Mathematical Methods of Physics, Vol. 1. Wiley, New York, p. 73.

Gaudett, M.A., Scully, J.R., 1994. Applicability of bond percolation theory to intergranular stress corrosion cracking of sensitized AISI 304 stainless steel. Metall. Mater. Trans. A 25, 775–787.

Hashin, Z., Shtrikman, S., 1962a. On some variational principles in anisotropic and nonhomogeneous elasticity. J. Mech. Phys. Solids 10, 335–342.

Hashin, Z., Shtrikman, S., 1962b. A variational approach to the theory of the elastic behavior of polycrystals. J. Mech. Phys. Solids 10, 343–352.

Hill, R., 1952. The elastic behavior of a crystalline aggregate. Proc. Phys. Soc. A 65, 349–354.

Hirth, J.P., Lothe, J., 1968. Theory of Dislocations. McGraw Hill, New York, pp. 400–409.

Hofmann, S., 1990. Surface analysis techniques in the study of segregation phenomena. Vacuum 40, 9–17.

Hutchinson, J.W., 1976. Bounds and self-consistent estimates for creep of polycrystalline materials. Proc. Roy. Soc. Lond. A 348, 101–126.

Juvinall, R.C., 1967. Engineering Considerations of Stress, Strain and Strength. McGraw-Hill Inc. New York, pp. 35, 55.

King, W.E., Schwartz, A.J., 1998. Toward optimization of the grain boundary character distribution in OFE copper. Scripta Mater. 38, 449–455.

Kroner, E., 1977. Bounds for effective elastic moduli of disordered materials. J. Mech. Phys. Solids 25, 137–155.

Kumar, M., King, W.E., Schwartz, A.J., 2000. Modifications in the microstructural topology in FCC materials with thermomechanical processing. Acta Mater. 48, 2081.

Larsen, U.D., Sigmund, O., Bouwstra, S., 1997. Design and fabrication of compliant micromechanisms and structures with negative Poisson's ratio. J. Microelectromech. Systems 6, 99–106.

Lehockey, E.M., Palumbo, G., 1997. On the creep behaviour of grain boundary engineered nickel. Mater. Sci. Eng. A 237, 168–172.

Lehockey, E.M., Palumbo, G., Grennenstuhl, A., Lin, P., 1997. Grain boundary engineered lead alloys [for battery electrodes]. In: Briant, C.L., Carter, C.B., Hall, E.L. (Eds.), Material Research Society Symposium Proceedings, Vol. 458. Materials Research Society: Pittsburg, PA, pp. 243–248.

Lin, P., Palumbo, G., Erb, U., Aust, K.T., 1995. Influence of grain boundary character distribution on sensitization and intergranular corrosion of alloy 600. Scripta Metall. Mater. 33, 1387–1392.

Mason, T.A., Adams, B.L., 1999. Use of microstructural statistics in predicting polycrystalline material properties. Metall. Mater. Trans. 30A, 969–979.

Midha, A., Norton, T.W., Howell, L.L., 1994. On the nomenclature, classification, and abstractions of compliant mechanisms. J. Mech. Des. Trans. ASME 116, 270–279.

Muschik, T., Hofmann, S., Gust, W., Predel, B., 1989. Surface and grain boundary segregation in Ni–In studied under identical conditions with AES. Appl. Surf. Sci. 37, 439–455.

Pan, Y., Adams, B.L., Olson, T., Panayotou, N., 1996. Grain boundary structure effects on intergranular stress corrosion cracking of alloy X-750. Acta Mater. 44, 4685–4695.

Palumbo, G., King, P.J., Aust, K.T., Erb, U., Lichtenberger, P.C., 1991. Grain boundary design and control for intergranular stress-corrosion resistance. Scripta Metall. Mater. 25, 1775–1780.

Palumbo, G., Aust, K.T., 1995. Solute effects in grain boundary engineering. Can. Metall. Quart. 34, 165–173.

Paul, B., 1960. Prediction of elastic constants of multiphase materials. Trans. Metall. Soc. AIME 218, 36–41.

Powell, B.D., Woodruff, D.P., 1976. Anisotropy in grain boundary segregation in copper-bismuth alloys. Philos. Mag. 34, 169–176.

Randle, V., Brown, A., 1989. Development of grain misorientation texture, in terms of coincident site lattice structures, as a function of thermomechanical treatments. Philos. Mag. A59, 1075.

Rockafellar, R.T., 1970. Convex Analysis. Princeton University Press, Princeton, p. 19.

Roe, R.J., 1965. Description of crystallite orientation in polycrystalline materials. III. General solution to pole figure inversion. J. Appl. Phys. 36, 2024–2031.

Sigmund, O., Torquato, S., 1996. Composites with extremal thermal expansion coefficients. Appl. Phys. Lett. 69, 3203–3205.

Sigmund, O., Torquato, S., Aksay, I.A., 1998. On the design of 1–3 piezocomposites using topology optimization. J. Mater. Res. 13, 1038–1048.

Sun, S., Adams, B.L., King, W.E., 2000. Observations of lattice curvature near the interface of a deformed aluminum bicrystal. Philos. Mag. A 80, 9–25.

Sutton, A.P., Balluffi, R.W., 1995. Interfaces in Crystalline Materials. Oxford Science Publications, Oxford, UK, pp. 12–20.

Was, G.S., Thaveeprungsriporn, V., Crawford, D.C., 1998. Grain boundary misorientation effects on creep and cracking in Ni-based alloys. J. Metals 50, 44–49.

Watanabe, T., 1984. An approach to grain-boundary design for strong and ductile materials. Res. Mech. 11, 47.

Watanabe, T., Murakami, T., Karashima, S., 1978. Misorientation dependence of grain boundary segregation. Scripta Metall. 12, 361–365.

Wells, D.B., Stewart, J., Herbert, A.W., Scott, P.M., Williams, D.E., 1989. The use of percolation theory to predict the probability of failure of sensitized, austenitic stainless steels by intergranular stress corrosion cracking. Corrosion 45, 645–660.

Willemse, M.W.M., Caspers, W.J., 1979. Electrical conductivity of polycrystalline materials. J. Math. Phys. 20, 1824–1831.

Yoshitomi, Y., Suzuki, S., Ueda, T., Tsurekawa, S., Nakashima, H., Hoshinaga, H., 1995. Grain boundary segregation in (110) symmetrical tilt bicrystals of an Fe–3%Si alloy. Scripta Metall. Mater. 32, 1067–1072.

Zeller, R., Dederichs, P.H., 1973. Elastic constants in polycrystals. Phys. Stat. Solidi B 55, 831–842.